Journal of the Department of Geography, Tourism and Hotel Management
54–1/2025

Original scientific article

CLIMATIC INFLUENCE ON THE LAKE DRAINAGE PROCESSES AND VEGETATION DYNAMICS IN ARID ECOSYSTEMS OF SOUTHERN AFRICA

Polina Lemenkova[A,B]

Received: October 3, 2024 | Accepted: April 25, 2025
DOI: 10.5937/ZbDght2501001L

ABSTRACT

Droughts and climate fluctuations can lead to seasonal drying in Etosha Lake, located in northern Namibia. Repetitive rises in temperature and lack of precipitation affect the hydrology and ecosystem health of using landscape of the Etosha Pan. Land cover dynamics of this salt ephemeral basin, located in Namibia, are subject to the climate and meteorological setting. To date, the spatiotemporal monitoring of this specific region of southern Africa, including the driving factors of salinity and the water cycle, and the drainage dynamics of the lake, remains unclear. The remote location of this area and the extreme desert climate make fieldwork in this region a challenge. Using a series of six multi-spectral Landsat 8-9 OLI/TIRS satellite images and cartographic products (CORINE and GEBCO for thematic and topographic mapping), we identify seasonal variations in the surface of the Etosha National Park affecting drainage events in the lake basin. Extreme heat periods (summer-early autumn) resulted in the drying of the basin, which was covered by the crust of salt and minerals, while wet periods in winter and early spring favour the growth of vegetation. Technically, this paper presents the use of the Machine Learning (ML) methods of GRASS GIS by libraries of Python Scikit-Learn for image classification by an ensemble learning approach with a Random Forest (RF) classifier. Land cover types were identified using ML modules of GRASS GIS and scripting techniques. The methodology of scripts is presented in the GitHub repository of the author. The results demonstrated seasonal landscape dynamics in Etosha Pan. The ML method of image classification proved to be an effective tool for monitoring changes in the landscapes of northern Namibia, Africa.

Keywords: *arid ecosystem; remote sensing; satellite image; scripting language*

INTRODUCTION

Etosha Pan is a unique, large, salty lake located in northern Namibia. It presents a vast basin in the land surface where water collects seasonally. Water availability here depends on rainfall and evaporation during dry periods, resulting in a surface covered by salt and mineral deposits. Recently, the lake experienced the effects of climate change and global warming. Warmer temperatures may have very distinct consequences for arid ecosystems, such as an increase in radial growth. This may depend on an insufficient water supply to com-

A Alma Mater Studiorum – University of Bologna, Department of Biological, Geological and Environmental Sciences (BiGeA), Via Irnerio 42, 40126 Bologna, Emilia-Romagna, Italy;
B Free University of Bozen-Bolzano, Faculty of Agricultural, Environmental and Food Sciences, Piazza Università, 5, IT-39100, Bolzano, South Tyrol, Italy;
polina.lemenkova2@unibo.it

pensate for the increased evapotranspiration in desert areas of southern Africa. Thus, moisture availability needs to be considered to predict the consequences of future climate change. Moreover, land overuse and soil degradation can lead to environmental problems in the southern regions of Africa. These include, for instance, soil erosion, landslides in the coastal areas along the Atlantic Ocean, rockfalls, increased water runoff in wadi or reduced water storage.

Namibia faces significant environmental challenges, including the drying of springs and the decline of biodiversity. All these climate-driven phenomena and related environmental processes have severe impacts on livelihoods in central and northern Namibia, even causing human deaths. However, there are still gaps in the understanding of water redistribution in ephemeral salty lakes, such as Etosha Pan, and its consequences for land-use management in northern regions of Namibia. Geospatial analysis of these areas would be useful for water policies and land management, with particular attention to the climate system in Africa.

The desiccation of springs and the decline of biodiversity. These climate-driven phenomena, along with associated environmental processes, have profound implications for livelihoods in central and northern Namibia, even contributing to human mortality. Despite these pressing issues, critical knowledge gaps persist regarding water redistribution in ephemeral salt lakes, such as the Etosha Pan, and its ramifications for land-use management in northern Namibia. A geospatial analysis of these regions could provide valuable insights for formulating effective water policies and land management strategies, with particular emphasis on the broader African climate system. This approach would enhance understanding of hydrological dynamics and support sustainable resource allocation in vulnerable ecosystems.

From an eco-hydrological point of view, this manuscript presents a numerical analysis of the eco-hydrology of the Etosha Pan salt lake in northern Namibia. Although the satellite data series has a short-term period (one calendar year), it contains diverse aspects to find effects between meteorological parameters (seasons of dry and wet periods) and characteristics of the lake as a response to the changing precipitation and temperature in the salt lake basin. In this way, this study presents a contribution to the eco-physiology of the lacustrine environment of the Etosha basin. Using Remote Sensing (RS) data, we studied the role of climate in environmental change in southern Africa.

So far, little is known about the frequency and influence of climate parameters and the role of temperature and precipitation in the water balance of Etosha. The remote location of this lake and the severe climate with extreme heat make fieldwork observation a challenge. In this regard, using RS data processed by ML methods presents an excellent tool for the environmental monitoring of African lake. Specifically, it explores the missing link between salt lake hydrology in northern Namibia with climate warming and vegetation coverage visible from space. Using satellite images, we explained seasonality in changes of salt and water in the lake through wet and dry periods and the presence of salt crust. Multiple studies applied GIS for remote sensing (RS) data processing earlier, which were considered in this work (Ousmanou et al., 2024; Zhang et al., 2023; Bakr et al., 2010). According to our study, seasonal temperature changes contribute much to the water balance of Etosha. Besides, precipitation interception and evapotranspiration partitioning in lacustrine coasts vary with periods and affect vegetation growth.

To maintain the water cycle, the coastal vegetation of Etosha has a significant ability to affect the water balance by absorbing water during wet days through the canopy and returning it to the sky as vapour. Though seasonal changes in precipitation and temperature have not been included in past water balance studies, this study revealed that fluctuations in dry-wet periods over the Etosha Pan basin combined with rainfall availability during the same period, such as mixed precipitation, contributed to higher throughfall, which in turn contributes to higher net precipitation (soil water recharge, in absence of runoff) and evaporative conditions inside the canopy of scarce vegetation, steppe and grasslands. We processed a series of satellite images, Landsat, to visualise the frequency of wet periods and dry episodes with respective changes in land cover types in the arid environment of northern Namibia.

Background

The use of Machine Learning (ML) has been at the centre of attention recently for the challenge of Earth observation data processing (Gupta et al., 2022; Deepthi Murthy et al., 2023; Lemenkova, Debeir, 2022, 2023; Yadav et al., 2022; Shahrin et al., 2020). ML has become an available approach in cartography along with advances in programming, and these methods are increasingly used in various tasks of environmental monitoring and mapping. The use of these tools ensures the automation of satellite data processing and supports operational monitoring using time series. Besides, it has an important effect on accuracy and the effectiveness of cartographic data processing. A high level of automation in ML-based data processing makes it possible to map land cover types rapidly and accurately (Jasiewicz, 2011).

In this regard, ML presents significant benefits and opportunities compared to the traditional cartographic methods possible using Geographic Information Systems (GIS) (Ayhan, Kansu, 2012; Lemenkova, 2024a). For instance, due to the introduced training and randomness in raster data processing ensured by computer-vision algorithms of automated image analysis, ML enables the avoidance of subjectivity in image classification. Various RS data can be used to detect and monitor land cover changes at local, regional and global scales. The goal of such studies aimed at change detection is to identify dynamics in land cover types using satellite images through their comparison between two or more dates. Such a method enables us to identify not only the type of changes but also to quantify their amount and extent (Goldblatt et al., 2018; Martínez-Montoya et al., 2010; Inzana et al., 2003).

Objectives and motivation

The RF approach was selected as a valuable method since it uses the computer vision approaches that have an anti-noise capacity, which is useful for image processing used for mapping changes in the basin from the evaporated to the flooding period. The coastal surroundings of the basin of Etosha Lake during dry periods are primarily covered by salt crust. This significantly affects the vegetation and only enables salt-tolerant species to grow in this region. While plant transpiration and soil evaporation can be measured directly through meteorological sensors and canopy chambers, evaporation from canopy interception can still only be estimated indirectly or modelled. For Namibia, the technical implementation of such fieldwork is challenging. To this end, RS data present a perfect tool for environmental monitoring.

There are still major uncertainties in the climate-environmental regulations of Namibia. For example, little is known concerning the rate of wet canopy evaporation during periods with high precipitation (rains and local floods). Estimated from fieldwork measurements or as the differences between precipitation and throughfall, such data could be useful for environmental and climate modelling of Namibia. In tropical ecosystems of Africa with a high and constant frequency of rains, the daily water budget may represent higher parts, which are suitable for vegetation growth. However, the relevance of precipitation and temperature for the water balance and vegetation coverage in arid areas and deserts such as northern Namibia is still largely unknown. Given the difficulties in fieldwork and the remote location of the study area, the RS data provide a contribution to our understanding of the climate-environmental-vegetation interactions in Namibia.

The arid landscapes of Namibia are influenced by meteorological settings and the seasonality of dry and wet periods. Precipitation supports the formation of convective clouds appearing over the lake in the winter, and thermal inversions, which lead to higher humidity over the lake and the occurrence of vegetation in coastal surroundings in the winter. The contrasting periods of dry summer create opposite conditions with a lack of precipitation, extreme temperatures and dried soil. As a consequence, the water balance in the lake is at an extremely low level, and a salt crust is formed. Such high variations in climate and precipitation at local scales affect the estimation of evaporation fluxes over the lake. In turn, this includes large uncertainties and is difficult to assess and interpret. The solar energy production potential of Namibia is high due to the intensity of heat for most of the calendar year. Nevertheless, key characteristics like cloud repeatability, salt crust thickness in Etosha, size of water decrease, coastal sediments and evaporated water content of the lake

are not observed. These are important parameters to assess the climate-environmental processes over Etosha that affect regional land cover types.

Structure and organization

The paper is organized as follows. After the Introduction, the following Chapter 2 describes the current state of the art in remote sensing data processing and the application of programming in geographical analysis. Chapter 3 presents the study area and provides a geographical and environmental background of the territory of Etosha. Chapter 4 presents the data used for spatial analysis. Chapter 5 explains the ensemble learning method with the RF approach to RS data processing. Specifically, the methodology provides snippets of GRASS GIS code. In Chapter 6, the results of image classification are presented and commented on. Chapter 7 discusses the obtained results and provides additional comments. Finally, Chapter 8 concludes the paper with a discussion regarding the landscapes and climate-related land cover changes in the Etosha Pan, northern Namibia.

State-of-the-art

In African climate studies, measurements of the land cover interactions with climate and water balance components are usually surrounded by considerable uncertainties. In environmental approaches to models, the oversimplifications are widely accepted. In the ecohydrology of arid regions, such as Etosha Lake. The latter is overcome by separating evapotranspiration into evaporation from surfaces inside the coastal lacustrine environment and transpiration by the vegetation. In view of this, the ensemble learning approach of image processing is the method of modelling that applies several learning paradigms to achieve accurate classification. The effects of this approach, resulting in the improved cartographic outputs approach, can be explained by the integrated power of different tools, which bring their benefits to the workflow compared to these algorithms when used alone.

In ML-based satellite image analysis, the ensemble learning includes a series of alternative models, such as RF or decision trees, ensuring a more adjusted workflow (Yoo et al., 2019; Singh et al., 2021; Mulik et al., 2023) or unsupervised (Shih, Chen 1994; Lemenkova 2023b, 2023c, 2023d; Lu et al., 2023) approaches to image classification. Moreover, the increased variability of images with different properties and resolution requires more advanced methods compared to the traditional approaches of image analysis that use pixel-based classification algorithms (dos Santos Luciano et al., 2019; Phiri et al., 2018; Dewali et al., 2023; Mao et al., 2020). This leads to the issues in accuracy and precision of the image classification process (Fisher et al., 2018; McKee, Weber 2021). Hence, Python algorithms of the Scikit-Learn library present a powerful instrument for ML, which has been investigated earlier (Adugna et al., 2022; Cuartero et al., 2022; Nguyen et al., 2019; Upadhyay et al., 2016). The RF algorithm embedded in the mapping of crop fields using Landsat imagery was thoroughly described in relevant works (dos Santos Luciano et al., 2021; Lemenkova, 2024b).

The satellite sensors provide the images of Earth's surface and present the collection of data suitable for monitoring landscape dynamics visible on the Earth's surface from space (Collins et al., 2020; Wei et al., 2020; Wang et al., 2022). Such data are valuable sources of information to evaluate trends in land cover changes over time when comparing multi-temporal datasets. For example, related works proposed an integrated application of the RF algorithms (Oliphant et al., 2019; Teluguntla et al., 2018; Ahmed et al., 2015), hazard risk assessment using fire mapping (Collins et al., 2020), urban sprawl analysis (Ghosh et al., 2014) and environmental monitoring of land cover types (Melville et al., 2018; Lemenkova, 2024c; Grinand et al., 2013). Therefore, satellite images were employed in this study for remote–sensing–based environmental mapping of northern Namibia. Further examples (Andreo et al., 2015; Strigaro et al., 2016; Rocchini et al., 2017) evaluated the use of GRASS GIS modules for geological mapping using satellite data.

The approach presented by De Sarkar et al. (2012) reports the links between GRASS GIS and Python and performs relatively well for environment monitoring using satellite imagery, but the proper scripts of GRASS GIS are not reported since the major point was using Python for launching GRASS GIS. Instead of unsupervised classification available in traditional software and clustering methods, GRASS GIS enables to collect the information on land categories with ML-based methods. This is a significant advantage of GRASS GIS since not all GIS have such ML tools available in the functionality. In this regard, GRASS GIS presents perspectives of using the advanced embedded ML methods, which can identify and record land cover classes on the satellite images covering Namibia in an Artificial Intelligence (AI)-based manner using computer vision techniques. As an alternative to the existing GIS methods, this article presents an application of advanced methods for image processing and classification using ML techniques of the gradient boosting algorithm implemented by GRASS GIS scripts (Hofierka et al., 2009; Lemenkova, 2023a, 2024d; Rocchini et al., 2013; Jasiewicz, Metz, 2011). The advantage of such an approach is that, unlike the existing conventional methods used in GIS, the ML-based classification is independent, which is achieved using computer vision. In this way, programming applies to the processing of geospatial data, which presents a multidisciplinary approach.

STUDY AREA

The study area is focused on the saline Etosha Pan (Figure 1).

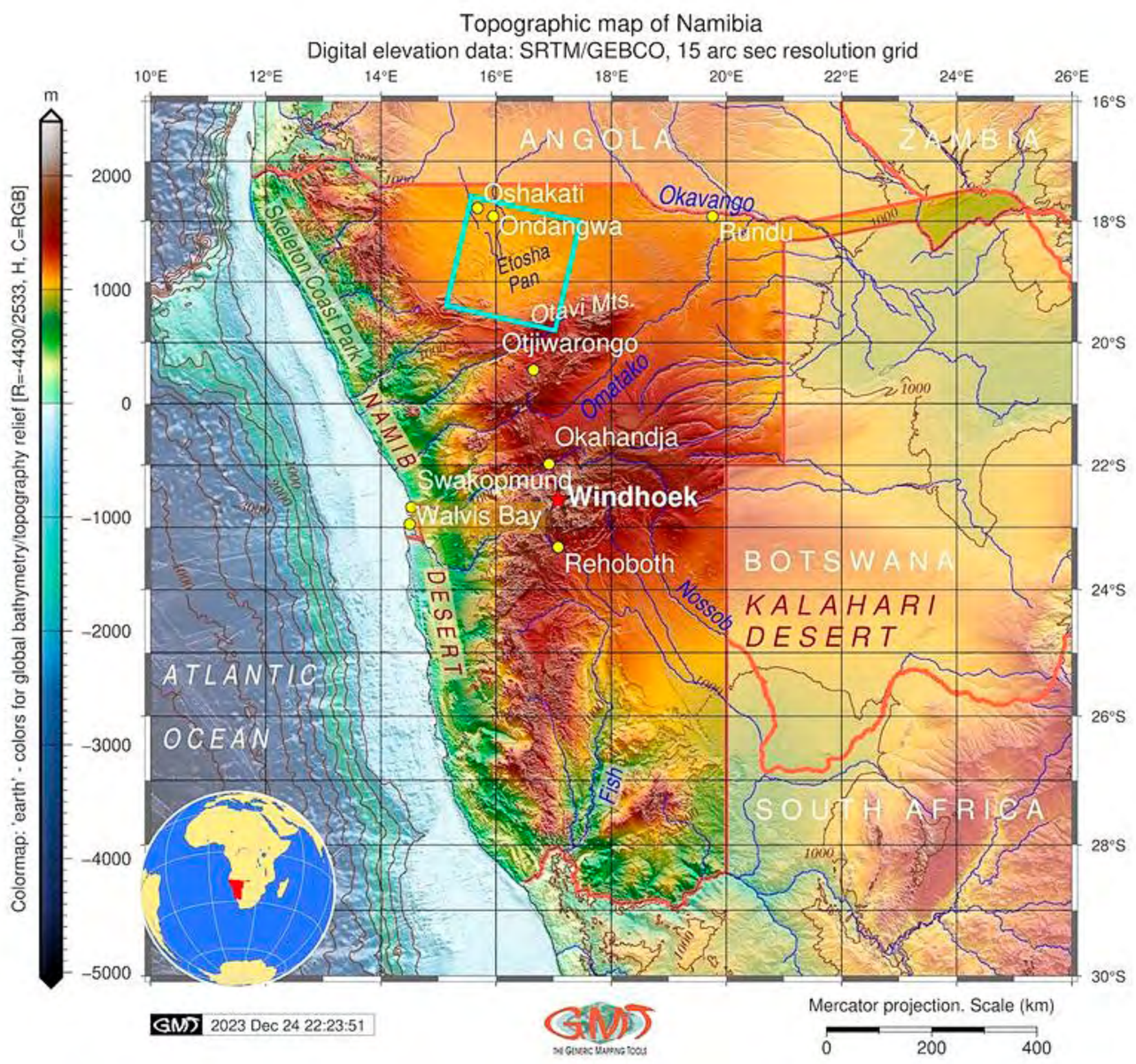

Figure 1. Topographic map of Namibia with indicated study area: Etosha Pan.
Mapping software: Generic Mapping Tools (GMT)

Source: Author (2024)

Etosha Pan belongs to the Cuvelai-Etosha Basin, a transboundary wetland area within the topographic depression located between southern Angola and northern Namibia. The basin was developed from the Palaeolake Etosha in the Tertiary and now presents a depression. It collects water from three drainage systems

from the Angolan highlands, the Cubango and the Cuvelai Drainage System (Miller et al., 2010). The topography of the region is flat, which causes the diurnal oscillation of wind and variations in thermo-topographical gradients (Preston-Whyte et al., 1994). Changing hydro-geomorphological setting of the deltaic drainage system of Etosha Pan leads to regular fluctuations in the water level, where the lake changes from a basin flooded by water to a completely dry pan covered by crust salt and minerals (Hipondoka et al., 2018).

Landscapes of the Etosha National Park are dominated by dry savannah, which is a typical land cover type of Namibia. Nevertheless, the variations of vegetation classes are highly fragmented, which depends on the inter-seasonal variety, and availability of moisture and correlates with the actual rainfall situation (Wagenseil, Samimi 2006), Figure 2. To preserve the resources of the vulnerable and fragile ecosystem of Etosha, nature conservation measures and policies were undertaken: the creation of the nature reserve of the Etosha National Park aimed at regulating the negative effects of agriculture activities, livestock husbandry, overgrazing, and tourism (Gargallo, 2020; Novelli, Gebhardt, 2007).

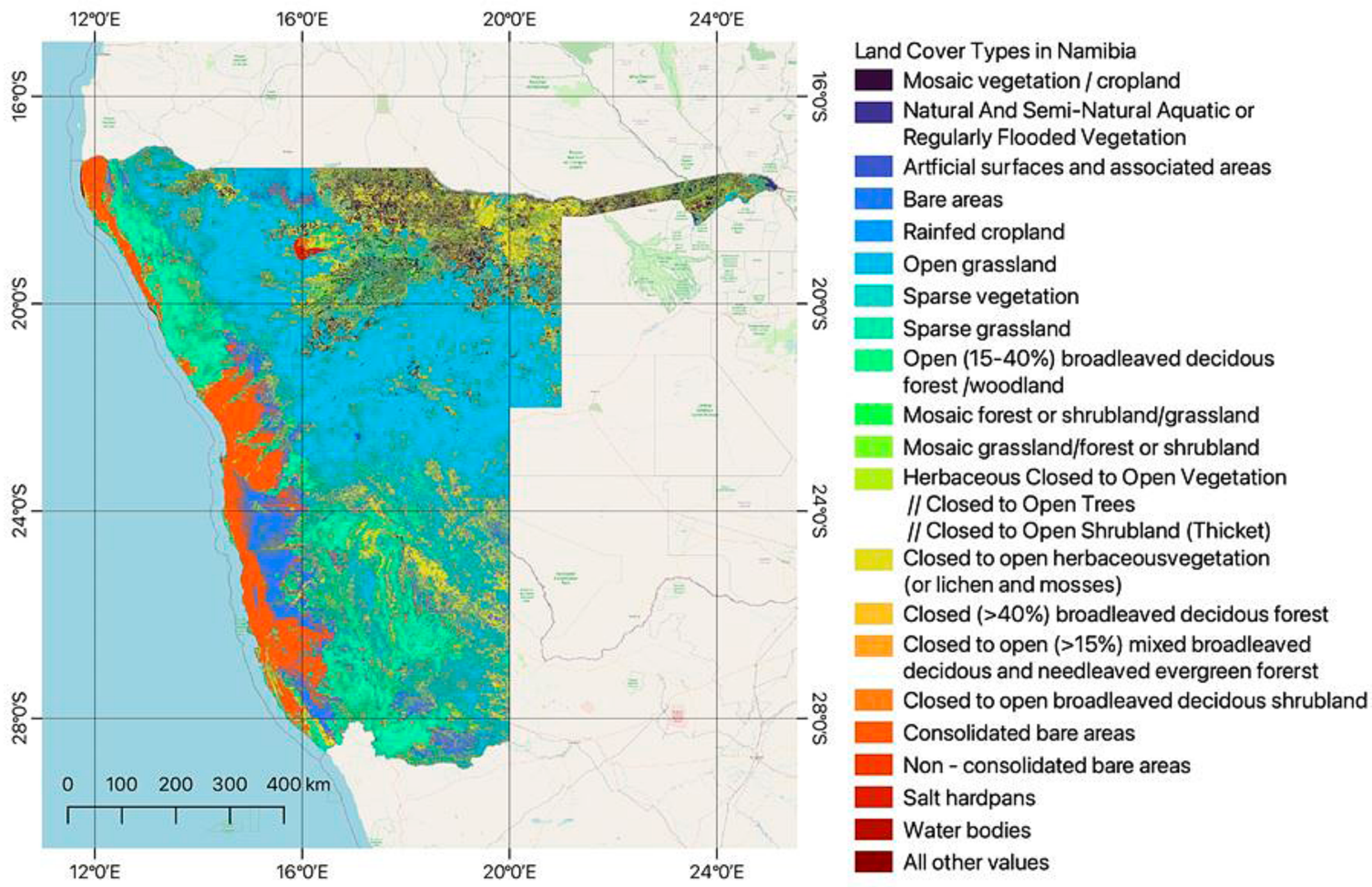

Figure 2. Land cover types of Namibia. Data source: Food and Agriculture Organization (FAO). Mapping software: QGIS

Source: Author (2024)

Oscillations in hydrological patterns from floods to complete desiccation indicate the progressively increasing aridity and desertification of the Etosha basin. This was affected by regional droughts, impacts from the Kalahari Desert and climate change. Two distinct seasons – dry from April to September and wet from October to March – divide climate and environmental patterns, while intra-seasonal water influx is unstable and depends on the ephemeral streams forming occasional pools (Himmelsbach et al., 2018). Climate-related hazards such as frequent and severe droughts, unstable water inflow and extreme temperatures typical for the arid and semi-arid climate of Namibia affect biodiversity. Rare species use Etosha as a shelter habitat during extreme heat (Luetkemeier et al., 2017). The ability of wetland birds such as flamingos to predict rain fronts and showers using changes in pressure gradients enables them to rapidly find water available in ephemeral reservoirs and pools of Etosha. As a result, migrating birds and rare species use the unique landscapes of Etosha as habitats during severe droughts in other regions (Fox et al., 1997; Roux, 1979; Berry et al., 2001; Simmons et al., 1999).

DATA

The data supporting the conclusions can be obtained from the publicly available USGS databases service of the satellite image repository: https://earthexplorer.usgs.gov/ The original images are shown in Figure 3. Technical characteristics that differ for each Landsat scene are provided in the CSV Table in the GitHub repository of the author: https://github.com/paulinelemenkova/Namibia_Etosha_GRASS_GIS_Ensemble_Learning

Besides, the major parameters are summarised in Table 1.

Table 1. Metadata of the satellite images Landsat 8-9 used in this study. The data were obtained from the EarthExplorer repository of the United States Geological Survey (USGS) and included six satellite images of the Landsat 8-9 Operational Land Imager and Thermal Infrared Sensor (Landsat 8-9 OLI/TIRS)

Landsat Scene Identifier	LC81790732022085LGN00	LC81790732022101LGN00	LC91790732022125LGN01	LC91790732022157LGN01	LC81790732022197LGN00	LC91790732022221LGN01
Date Acquired	2022/03/26	2022/04/11	2022/05/05	2022/06/06	2022/07/16	2022/08/09
Roll Angle	0.000	0.000	0.001	0.000	-0.001	0.000
Date Product Generated L2	2022/03/30	2022/04/19	2023/04/17	2023/04/14	2022/07/26	2023/04/03
Date Product Generated L1	2022/03/30	2022/04/19	2023/04/17	2023/04/14	2022/07/26	2023/04/03
Start Time	2022-03-26 08:55:28.788292	2022-04-11 08:55:30.641875	2022-05-05 08:55:23	2022-06-06 08:55:13	2022-07-16 08:55:54	2022-08-09 08:55:50
Stop Time	2022-03-26 08:56:00.558292	2022-04-11 08:56:02.411875	2022-05-05 08:55:55	2022-06-06 08:55:45	2022-07-16 08:56:26	2022-08-09 08:56:22
Land Cloud Cover	1.32	2.17	4.72	7.61	7.33	2.09
Scene Cloud Cover L1	1.32	2.17	4.72	7.61	7.33	2.09
Ground Control Points Model	655	731	757	770	770	764
Geometric RMSE Model	6.052	5.435	4.999	5.096	4.984	4.731
Geometric RMSE Model X	4.294	3.929	3.628	3.534	3.632	3.393
Geometric RMSE Model Y	4.265	3.755	3.440	3.671	3.413	3.297
Sun Elevation L0RA	52.82328395	49.80572103	44.79448536	39.50399786	39.59460724	43.81050644
Sun Azimuth L0RA	58.84443485	50.14840089	40.94078960	36.09442691	38.72515388	43.52123333
TIRS SSM Model	FINAL	FINAL	N/A	N/A	FINAL	N/A
Satellite	8	8	9	9	8	9
Scene Center Lat DMS	"18°47′15.47""S"	"18°47′14.60""S"	"18°47′14.57""S"	"18°47′14.42""S"	"18°47′15.50""S"	"18°47′15""S"
Scene Center Long DMS	"16°19′24.89""E"	"16°16′36.80""E"	"16°17′21.16""E"	"16°17′26.23""E"	"16°18′50.76""E"	"16°16′07.28""E"
Corner Upper Left Lat DMS	"17°44′22.85""S"	"17°44′23.03""S"	"17°44′22.99""S"	"17°44′22.99""S"	"17°44′22.88""S"	"17°44′23.06""S"
Corner Upper Left Long DMS	"15°13′38.35""E"	"15°10′55.38""E"	"15°11′36.13""E"	"15°11′36.13""E"	"15°13′07.79""E"	"15°10′24.82""E"
Corner Upper Right Lat DMS	"17°43′30.40""S"	"17°43′32.48""S"	"17°43′31.87""S"	"17°43′31.87""S"	"17°43′30.76""S"	"17°43′32.74""S"
Corner Upper Right Long DMS	"17°24′09.43""E"	"17°21′16.42""E"	"17°22′07.28""E"	"17°22′07.28""E"	"17°23′38.90""E"	"17°20′56.04""E"
Corner Lower Left Lat DMS	"19°51′06.55""S"	"19°51′06.73""S"	"19°50′56.94""S"	"19°50′56.94""S"	"19°51′06.59""S"	"19°50′57.01""S"
Corner Lower Left Long DMS	"15°13′48.61""E"	"15°11′03.59""E"	"15°11′44.84""E"	"15°11′44.84""E"	"15°13′17.69""E"	"15°10′32.63""E"
Corner Lower Right Lat DMS	"19°50′07.33""S"	"19°50′09.71""S"	"19°49′59.27""S"	"19°49′59.27""S"	"19°50′07.76""S"	"19°50′00.24""S"
Corner Lower Right Long DMS	"17°25′57.86""E"	"17°23′02.69""E"	"17°23′54.06""E"	"17°23′54.06""E"	"17°25′26.94""E"	"17°22′41.92""E"
Scene Center Latitude	-18.78763	-18.78739	-18.78738	-18.78734	-18.78764	-18.78750
Scene Center Longitude	16.32358	16.27689	16.28921	16.29062	16.31410	16.26869
Corner Upper Left Latitude	-17.73968	-17.73973	-17.73972	-17.73972	-17.73969	-17.73974
Corner Upper Left Longitude	15.22732	15.18205	15.19337	15.19337	15.21883	15.17356
Corner Upper Right Latitude	-17.72511	-17.72569	-17.72552	-17.72552	-17.72521	-17.72576
Corner Upper Right Longitude	17.40262	17.35456	17.36869	17.36869	17.39414	17.34890
Corner Lower Left Latitude	-19.85182	-19.85187	-19.84915	-19.84915	-19.85183	-19.84917
Corner Lower Left Longitude	15.23017	15.18433	15.19579	15.19579	15.22158	15.17573
Corner Lower Right Latitude	-19.83537	-19.83603	-19.83313	-19.83313	-19.83549	-19.83340
Corner Lower Right Longitude	17.43274	17.38408	17.39835	17.39835	17.42415	17.37831

Salinisation of the Etosha Pan is caused by seasonal fluctuations from dry to wet periods. During the hot summertime, rains gradually slow and cease, leaving the basin of the lake covered by a crust of salt and minerals. Parched brownish landscapes in the western and central parts of the lake clearly contrast with the remaining segments of the lake, still filled with water. Such changes are visible in the images in Figure 3, where different colours of water varying from electric cyan to dark navy blue show the depths of the lake, with darker shadows indicating deeper segments. The location of the wettest and deepest topographic areas in the eastern part of the basin well represents the local climate setting of the Etosha, where mean annual rainfall ranges from 250 mm/year in the west and up to 550 mm/year in the east (Koeniger et al., 2021). Green colours indicate mosaic vegetation in the surrounding landscapes (Figure 3).

Major technical characteristics of the satellite images common for all the scenes are as follows: Landsat Collection Category – T1, Collection Number 2, Data Type L2 – OLI_TIRS_L2SP; Sensor Identifier – OLI/TIRS; Station Identifier – LGN. The images were taken during the day period with nadir on at Worldwide Reference System (WRS) Path 179, WRS Row – 73 of the Landsat satellite. Product Map Projection L1 for all the scenes is Universal Transverse Mercator (UTM) Zone 33 for northern Namibia, with Datum and Ellipsoid – WGS84. The Ground Control Points (GCP) Version for all the images is 5. The images were preprocessed by the provider using Landsat Product Generation System (LPGS) Processing Software Version 15.6.0 for Landsat-8 and 16.2.0 for Landsat-9 scenes. Technically, the LPGS generates the data products of Landsat in GeoTIFF output format using standard image parameters, using the Cubic Convolution (CC)

resampling method and 30-m resolution in most of the spectral bands and a spatial coverage of 185 km swath for each scene.

The dataset illustrates the environmental changes in Etosha Pan that fluctuate from the wet period, when the lake is filled with water, to the dry period, when the basin becomes covered with a salt crust. On the set of false colour and natural colour composites of images shown in Figure 4, the bright colours of the remaining water and a thin channel connecting the deep part of the basin with a drying segment filled with salt and minerals offer a clear contrast with the parched brownish landscapes of the surrounding savannah. In the dry months (June to August), the bare soil areas contrast with the images in the wet season (March to May), with areas covered by lush vegetation.

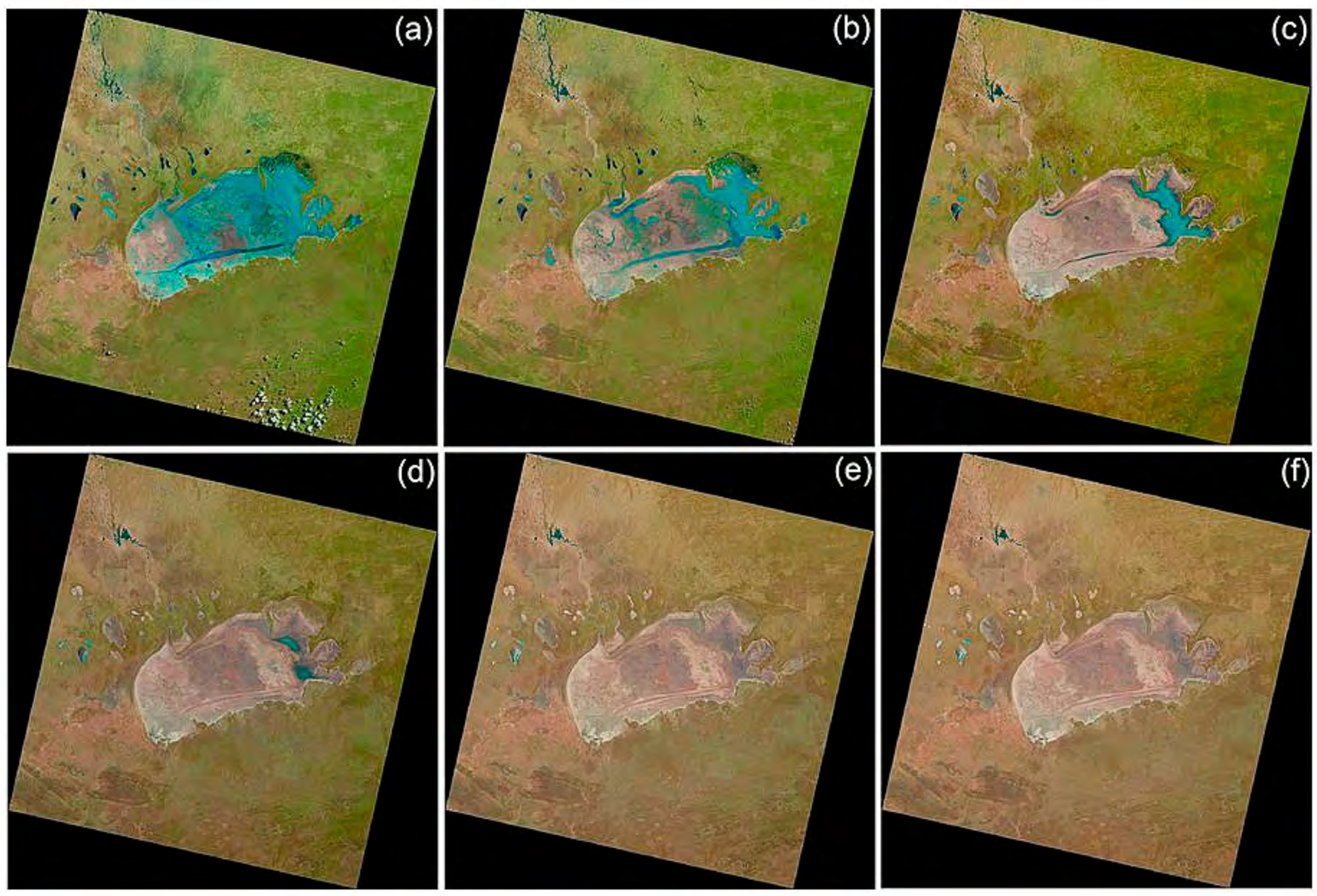

Figure 3. Landsat 8-9 OLI/TIRS images used as dataset obtained from the USGS covering the Etosha Pan region, Namibia, 2022: (a): 26 March; (b): 11 April; (c): 5 May; (d): 6 June; (e): 16 July; (f): 9 August. The images are shown in RGB colours

Source: Author (2024)

METHODS

The brief description of the workflow is as follows. During image processing, the Landsat images are computed by GRASS GIS software, which presents a powerful toolset for image analysis (GRASS Development Team, 2022). The scripts used for image processing for six satellite images are provided in the GitHub repository of the author: https://github.com/paulinelemenkova/Namibia_Etosha_GRASS_GIS_Ensemble_Learning.

The Generic Mapping Tools (GMT) (Wessel et al., 2019) is adopted to map topographic information and visualise the location of the study area using the overlaid extent of the multispectral Landsat images, Figure 1. More specifically, the GMT was used using scripting techniques reported and described in earlier works (Lemenkova, 2022a, 2022b). The year 2022 was selected because of the quality and availability of the satellite images without clouds, and of excellent quality. The data were only used for one year to monitor seasonal changes. The QGIS software was used for land cover mapping to represent geospatial information of the landscapes in northern Namibia. Figure 1 was plotted using Generic Mapping Tools (GMT) scripts using GEB-

CO-2023 data. Figure 2 was created using QGIS using FAO data. Figures 3 to 7 were created using the GRASS GIS scripts using processed satellite images Landsat 8-9 OLI/TIRS, USGS.

The GRASS GIS ML framework of image processing described below was employed to map seasonal variations in the Etosha Pan using six satellite multispectral Landsat 8-9 OLI/TIRS images within one month. Image analysis was performed on Landsat scenes taken in different time spans from April to August, where the texture of land cover types is highly diversified due to the natural processes of water evaporation from the basin and drying lakes. The detected landscape dynamics enabled to demonstration of the robustness of the RF-based classification method to monitoring seasonal variations using Earth observation data. Moreover, several colour composites were generated using the GRASS GIS module 'r. Composite' since such band combinations of the multispectral images detail features on the land surface and provide more information compared to the monochrome bands taken separately.

The performance of both the RF and MaxLike methods of image classification was visualised, compared and evaluated with six 30-m resolution multi-spectral Landsat OLI-TIRS multispectral satellite images with the results shown as colour-classified images in Figure 5 and Figure 7. The class distribution of pixels in the original multispectral colour images was computed and summarised by the module of GRASS GIS in the statistical report for each image.

Colour composites were generated for the classification approach based on information on pixel reflectance derived automatically using computer vision algorithms during the classification processes for maximum likelihood and random forest algorithms, respectively. We used the class separability matrix for the extraction of pixels according to the computed feature classes using several iterations. The number of stable points was computed for each image, and the convergence represented more than 98% for each scene. The signature file for each image was generated using data on spectral signatures which measures the similarity of pixels Digital Numbers (DN) for assignment to classes. This approach was applied to the whole classification process during the MaxLike procedure. Training cluster maps were computed for 10 classes of land cover types over the study area. We computed the classes using the clustering methods followed by the MaxLike algorithms and got the seed for the next step of the Random Forest (RF) algorithm which labelled these pixels assigned to different classes to obtain the classified map in GRASS raster format.

As demonstrated in this work, image analysis ties climate parameters (seasonality during dry and wet periods) and environmental responses (land cover types) to the relationship that contributes to the positive feedback between vegetation and weather in Namibia. Thus, image analysis represents a technical link in the positive feedback loop in studies that focus on revealing correlations between climate and ecology. The RF function algorithm of ensemble learning was derived from the embedded Python library of Scikit-Learn and used to test the simulation of the satellite image time series in the Etosha Pan region of Namibia. The trained pixels were obtained from the 'RandomForestClassifier' algorithms connected to the Scikit-Learn libraries of Python (Pedregosa et al., 2011) embedded with the GRASS GIS ML function of image analysis. The RF is a type of bagging algorithm of image classification that uses the Machine Learning (ML) methods of the classification and regression tree decision as learners. The randomness of data points in a raster image evaluated in this algorithm is assessed for reducing model variance. As a result, the advantages of the RF consist of an excellent generalization approach to data classification which combines the results of multiple decision trees to reach a single classification result through anti-overfitting.

In the process of RF refinement, the following procedures were completed using a supervised learning model 'RandomForestClassifier'. First, training areas were created from the 'training map' where the results of the clustering raster map with labelled pixels assigned to 10 classes were used as balanced training data using class weights. Such adjustment enabled us to automatically refine weights inversely proportional to class frequencies of pixels in each raster of the classified Landsat image. Second, the standardised feature variables were converted into values of zero mean and unit variance to reduce the complexity of the computations. Next, the classification results (Figure 7) show that spectral distributions of the pixels discriminated some regions within the Etosha Pan more precisely compared to the MaxLike and clustering approaches. The class probabilities were predicted using the 'r.learn.predict' module. Third, feature importances were com-

puted using permutations of pixels, which were placed in a discrete raster around the boundary study area to increase the accuracy of computation.

RESULTS

In this study, we quantified the capacity of the land cover types around the Etosha basin to reflect changes in the water level of the lake, and we provided a series of maps made using image classification in the two different seasons, dry season in summer-autumn months, and wet season during winter-spring periods. From the botanical point of view, the higher water storage capacity of the vegetation depended on the leaf area index (LAI), which depended on the key climate parameters (precipitation, temperature, evapotranspiration). Land cover types around Etosha, typically represented by savanna woodlands, grasslands, and shrublands, were relevant for the water cycle in this region and demonstrated seasonal changes on the satellite images for each classified event. The results of the present study present maps generated based on the classified series of satellite images Landsat 8-9 OLI/TIRS on the Etosha saline pan. These maps evaluated the dynamics of the salt crust and seasonal reserve of water in the Etosha, Figures 5, 6 and 7.

The relevance of the capacity of plants to hold water was particularly high and visible on the satellite images in transitive periods (images in March and August) when precipitation was changing (reflecting seasonal climate variability in Namibia). In this case, the water was used to refill the canopy of scarce trees and plants in grassland and savannah, as well as groundwater in soil reservoirs, without being lost as runoff. This large amount of water intercepted by the canopy, savannah and grasslands reflects the precipitation that was captured by the leaves of vegetation. Locally, water was re-emitted as evaporation, thus changing the humidity around the lake. In turn, this favoured the formation of the crystalline coverage of salt crust along the coasts of the Etosha Pan.

The comparative analysis of images presented by the Landsat time series illustrated the process of water evaporation and its gradual replacement by salt and minerals during a calendar cycle from wet to dry periods

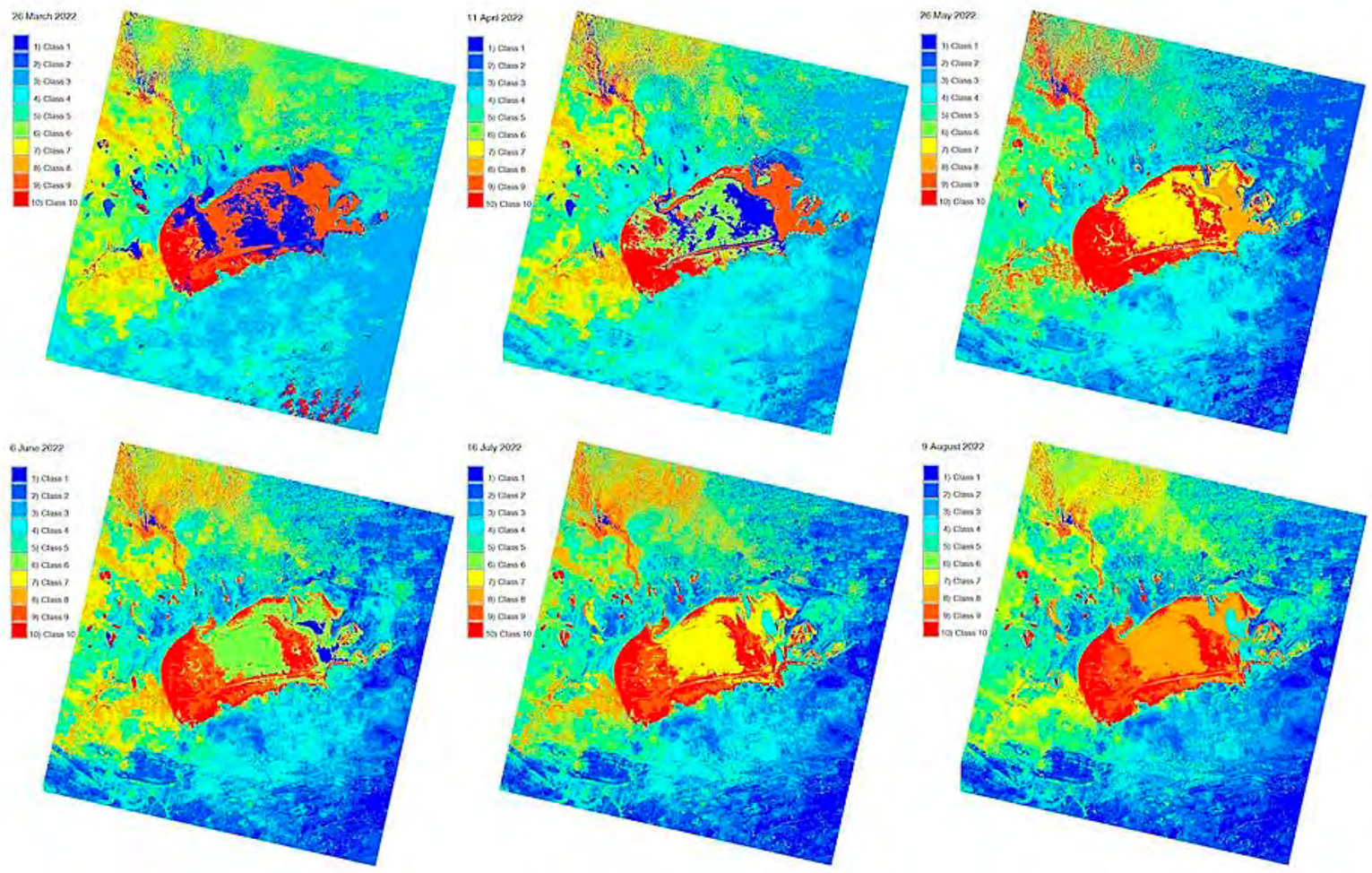

Figure 4. Classification of the Landsat-8-9 OLI/TIRS images covering the Etosha Pan region, Namibia using the 'MaxLike' method: (a): 26 March 2022; (b): 11 April 2022; (c): 5 May 2022; (d): 6 June 2022; (e): 16 July 2022; (f): 9 August 2022

Source: Author (2024)

in Namibia. Technically, the maps show the effectiveness of the novel module of GRASS GIS, which is based on ensemble learning by RF algorithms. We investigated the effects of several approaches to image classification using maximal likelihood (MaxLike) and random forest (RF) algorithms, i.e. the traditional pixel-based and object-based approaches. The comparison enabled optimisation for the image processing workflow using a series of modules, including the ML components integrated with the Scikit-Learn package of Python.

Figure 4 shows the classification results for different images taken from the wet period (March to May) and the dry period (June to August) using band combinations of Landsat 8-9 OLI/TIRS. The 10 generalized land cover classes include the following types detected and identified using the maximal likelihood approach as a seed for the next random forest approach: 1) Mosaic vegetation/cropland 2) Aquatic or regularly flooded vegetation; 3) Bare areas and artificial surfaces; 4) Mixed broadleaved deciduous forests; 5) Open grassland; 6) Rainfed cropland; 7) Salt hardpans; 8) Water bodies (Etosha basin and other lakes); 9) Herbaceous vegetation, shrubland and thickets; 10) Sparse savannah grasslands.

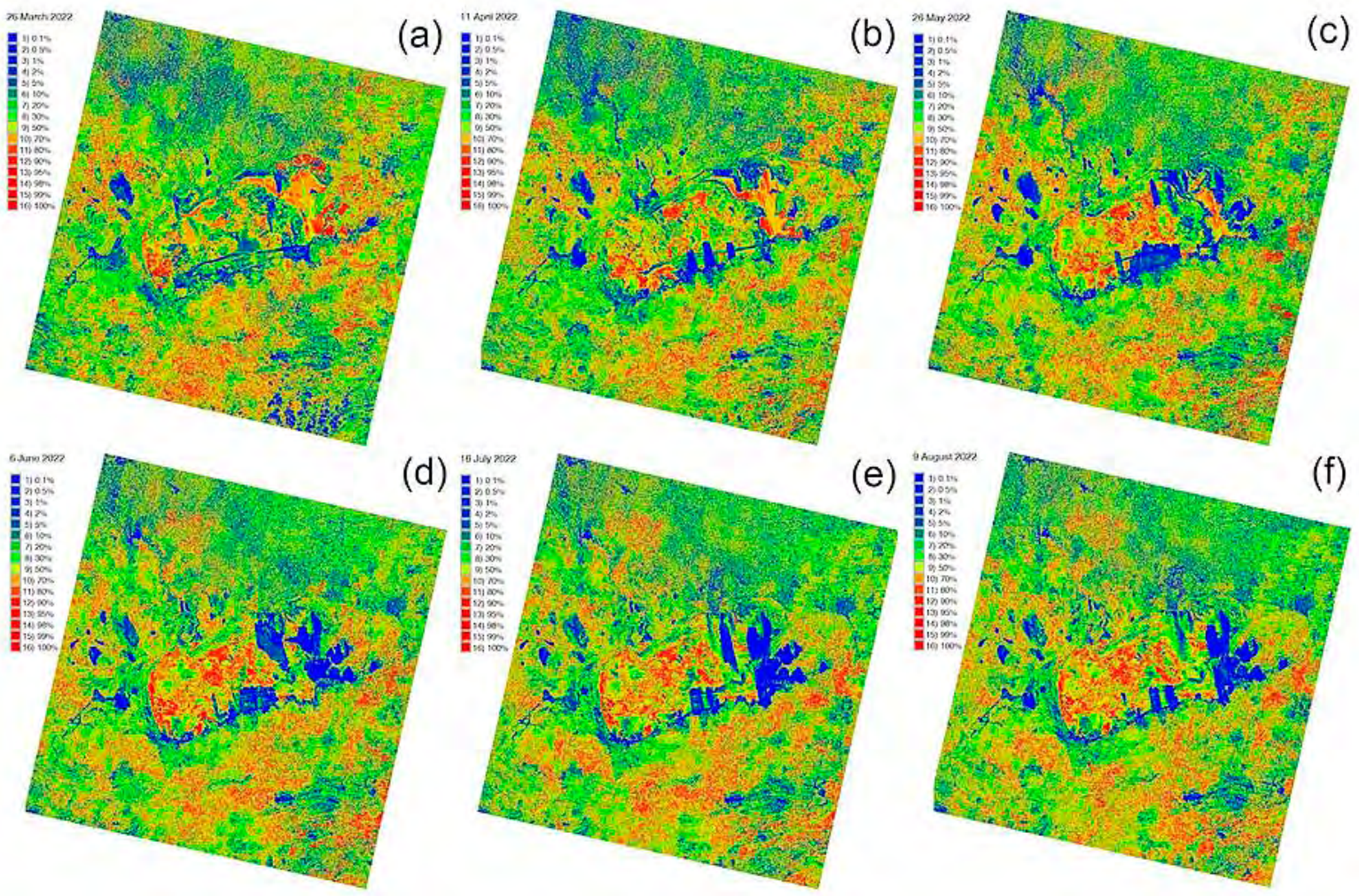

Figure 5. Accuracy assessment using the rejection probability for pixels classified for Landsat-8-9 OLI/TIRS images on the Etosha Pan region, Namibia: (a): 26 March 2022; (b): 11 April 2022; (c): 5 May 2022; (d): 6 June 2022; (e): 16 July 2022; (f): 9 August 2022

Source: Author (2024)

The accuracy analysis is demonstrated in Figure 5, which shows the rejection probability for classified pixels. The explanation of the accuracy assessment (Figure 5) is as follows. The pixel elements in the rows of the raster image show the pixels that are correctly classified by this algorithm approach with regard to the ground truth. Divided by the total number of pixels on the study area assigned to the category of the land class corresponding to these pixels, represents the amount of correctly classified cells recognised by the algorithm and identified correctly. Hence, this approach describes the confusion and correspondence between the target land cover class identified on the satellite image and the corresponding land cover category on the CORINE raster map. This comparison identifies the chance that a cell that has been assigned to a particular land cover category belongs in reality to the same class. The cluster parameters used for evaluating the spectral similarity of the adjacent classes were computed by the statistical reports generated by GRASS GIS during classification. The number of initial classes was set to 10 according to the major land cover types in the Etosha Pan basin and used to calculate the percentage convergence for each image. Other statistical values included minimum class size, class separation for each image, and sampling interval. The standard deviations and means for seven bands of imag-

es were used to evaluate the weights of the spectral reflectance of pixels and texture features. The initial means for each band of the textured mosaic were computed for each image.

The RF classification demonstrated in Figure 6 was calculated based on the classification (MaxLike) as seed data in the previous step and yielded more robust and better results compared to the MaxLike. The landscape patches are more diversified and fragmented into smaller polygons within and beyond the lake basin (Figures 5 and 7). Compared to the performance of 'MaxLike', the Random Forest classifier performed better in the case of similar classes in terms of separability of adjacent landscape patches. For instance, the grasslands, salt hardpan area of Etosha and flooded areas are clearly distinct from the mosaic trees and regions of broadleaved deciduous forests due to the different texture characteristics and spectral reflectance of pixels. These classes were more easily segmented compared to the areas with similar parameters, such as 'sparse savannah grasslands', compared to classes 'herbaceous vegetation, shrubland and thickets'. The distributions of pixels according to spectral reflectance can only discriminate those regions that have distinct characteristics of brightness.

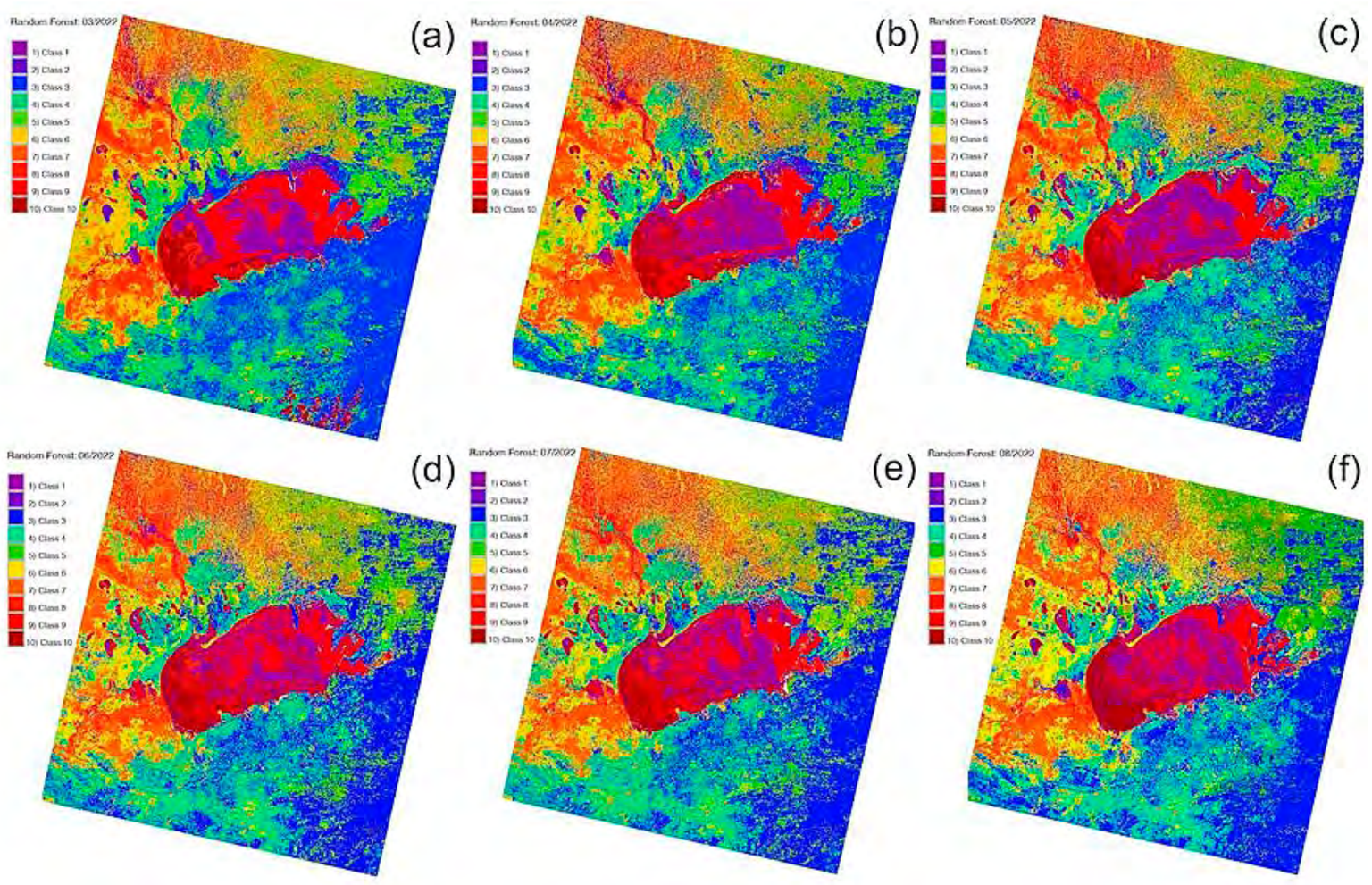

Figure 6. Results of the Random Forest (RF) classification using ML approach of GRASS GIS for the Landsat-8-9 OLI/TIRS images on Etosha Pan, Namibia: (a): 26 March 2022; (b): 11 April 2022; (c): 5 May 2022; (d): 6 June 2022; (e): 16 July 2022; (f): 9 August 2022

Source: Author (2024)

As shown in Figure 6, the distribution of spectral characteristics of diverse land cover types is affected by seasonal changes, which are integrated with the effects of salinisation of the basin in dry periods from May onwards. RF yielded better results compared to the traditional classification using MaxLik, Figures 5 and 6. The performance of RF was further evaluated with several processed images. Thus, the ML model was trained, and its performance was investigated using a non-random data partition approach to image classification. Instead of this algorithm that splits the image into segments, the RF algorithm organised the raster image into different classes according to the land cover types around Etosha and then processed each scene using a training dataset obtained from the unsupervised automatic clustering. The results of RF classification are better compared to the unsupervised classification (Figure 7. Despite the occasional pixel misclassification in some regions of the central basin where the over-fragmented mosaic of patches is visible, the overall accuracy is higher. In general, the RF approach outperforms unsupervised clustering due to technical improvements: ensemble learning is based on the adaptive integration of land cover features based on automated recognition of spectral properties of pixels constituting raster scenes.

DISCUSSION

In this study, we show that the effects of climatic seasonal fluctuations influence the land cover coverage in the protected areas of Etosha National Park. This particularly affects the climate-driven setting, i.e. seasonal changes in ephemeral lakes. These variations were detected using the classification of a short-term series of satellite images taken during one year. Compared with previous studies on the environment of Namibia, we presented several maps that demonstrate the decrease in water supply and increase in salinity in summer periods, respectively. The dry period with low water availability necessarily affects vegetation, which changes, as is visible on the satellite images taken in the early autumn period.

This effect of seasonality in salinity and water content in the arid lake of Etosha is mediated by coastal land use by locals and habitats for animals. Hence, the cumulative effects on the landscape are due to the climatic and anthropogenic processes. Specifically, in areas largely surrounded by dry salty coasts, water scarcity increases after periods of low availability of precipitation and an increase in temperature, i.e. during summer. In contrast, the greenness notably increases in the early spring period and during winter due to the increased precipitation. These fluctuations are clearly visible on the processed and classified images. Thus, in this study, we trained an ML classification model using GRASS GIS for mapping and visualisation of the lake drainage process during one calendar year to stress the seasonality of these processes. We utilized embedded libraries of Python (Scikit-Learn) for machine learning data processes, such as the ensemble learning algorithms described above.

Among the tested algorithms, Random Forest (RF) supervised classification and MaxLike unsupervised classification methods were compared and discussed for model training. The results demonstrated that ML has several advantages: it effectively handles heterogeneous satellite data that include raster pixels representing both continuous and categorical variables, and it demonstrates tolerance against outliers within raster matrix cells. Finally, ML algorithms of image processing generate improved models with reduced errors and bias, which outperform unsupervised training models.

The results show that satellite-derived information for the detection of salt lake extent and the detection of drainage events on the short-term time series of the images in the arid environments of north Namibia presents a technical challenge. This is because of the spectral properties of similar land cover types and salts that can be misidentified due to chlorophyll concentration. Besides, coastal areas have diverse salt crusts and suspended solids in shallow water, which also leads to pixel misclassification. In such difficult tasks, ML methods of Python-based identification of land patches and pattern recognition ensured accurate results of image processing, coloured dissolved organic matter, water depth, and observation conditions.

CONCLUSION

A novel hybrid ensemble learning ML method of GRASS GIS for image classification is presented and proposed for satellite image processing for analysis of the changing environmental setting of the Etosha Pan, located in northern Namibia. This includes three major approaches which were tested and evaluated in this study: clustering with generating training pixels, traditional classification using a maximum likelihood approach and Random Forest (RF) classification of ML. Additionally, colour composites were created using band composites of Landsat. The classification accuracy was computed using the confidence level of pixels assigned into ten land cover classes around the Etosha Pan. The RF algorithm provides the output of multiple decision trees to reach a classification of the satellite image. Thus, the hybrid classifier of the prediction pattern evaluates the assignment of pixels on a raster scene using multiple decision trees.

The efficiency of environmental mapping that operates with satellite images, especially for monitoring seasonal fluctuations in land cover types, can now be improved by using the Machine Learning (ML) methods of Python integrated with cartographic tools. We used raster pixels as samples for model training and

automated testing of classification performance. To this end, we used the Python-based Scikit-Learn library to fit models in GRASS GIS software. Comparison of several algorithms enabled to finding of the optimal model (Random Forest, RF) and adjustment parameters of 10 land cover classes over Etosha Lake through a random search of cross-validated pixels. Using such an approach, the analysis of scenes indicated evaporated water during dry periods, which coincides with the cycle of flooding and evaporation in northern Namibia. During the dry period, a mineral-encrusted salt pan covers the surface of the basin, which reaches its peak in August, while the most water-filled period is in March.

The comparison of these scenes as ML-classified satellite images shows gradual development in the salinisation of the Etosha Pan basin during six consecutive months in 2022. The results demonstrate that RF has high automation in image processing, accuracy in pixel assignments, and increased details of classification with more fragmented identified patterns in the landscapes of northern Namibia. The findings indicate that the proposed RF algorithms of the ensemble learning methods of GRASS GIS are dominant in comparison with other methods. Thus, it demonstrates fast processing when dealing with multi-spectral images using RS modules, 'r.learn.predict' and 'r.category' and complex hybrid functions of 'r.learn. RF shows its excellent exploration of the training dataset used as a seed. The extensibility of RF is represented in optimising training pixels derived from the generated dataset by the 'r.random' module with different heterogeneity of the landscapes that are expressed in the fragmentation of patches. Besides superior performance, the time complexity of RF when used in GRASS GIS is acceptable compared with the 'MaxLike' approach using the 'i.maxlik' module as a traditional variant of image classification. While traditional classification methods are usually based on Geographic Information Systems (GIS) tools, a novel tool of Machine Learning (ML) presents a more effective, automated and accurate approach to image processing. The following summarizing remarks can be added to the conclusion:

- Etosha Pan is a large salt pan in northern Namibia, which is a vast basin on the land surface where water collects seasonally. Water availability depends on rains and evaporates during dry periods, with the surface covered by salt and minerals. Landsat 8-9 OLI/TIRS images present a perfect data source for the identification of seasonal oscillations in water and salt levels in the saline Etosha Pan.
- The ensemble learning approach by the Random Forest algorithm is applied for the automated classification of remote sensing (RS) data.
- Classification of RS data presents an effective method for monitoring these changes using a comparison of several scenes collected during dry and wet periods.

This study contributed to the environmental monitoring of Etosha Pan through the analysis of satellite images. Time series analysis visualised the dynamics of droughts in southern Africa. Such environmental monitoring supports preserving the ecosystem of Etosha National Park in Namibia, where rare species depend on the availability of water. For example, elephants, lions and rhinos have to adapt to the seasonal changes of water. As the technologies develop along with the programming algorithms, cartographic modelling and data analysis are notably improved in many implementations. Integrated cartographic and ML tools deal with the creation of maps using the results of satellite image classification and processing that are used for environmental monitoring, evaluation, data mining and retrieval of geospatial information.

ABBREVIATIONS

- Cubic Convolution – CC
- General Bathymetric Chart of the Oceans – GEBCO
- Geographic Information Systems – GIS
- Geographic Resources Analysis Support System – GRASS
- Ground Control Points – GCP

- Generic Mapping Tools – GMT
- Landsat Operational Land Imager and Thermal Infrared Sensor – Landsat OLI/TIRS
- Landsat Product Generation System – LPGS
- Food and Agriculture Organization – FAO
- Object-Based Image Analysis – OBIA
- Random Forest – RF
- Remote Sensing – RS
- United States Geological Survey – USGS
- World Geodetic System 1984 – WGS84
- Worldwide Reference System – WRS

REFERENCES

Adugna, T., Xu, W., Haitao, J., Fan, J. (2022). Comparison of FY-3C VIRR and MODIS Time-Series Composite Data for Regional Land Cover Mapping of a Part of Africa. *IGARSS 2022 - 2022 IEEE International Geoscience and Remote Sensing Symposium*, 3163-3166. https://doi.org/10.1109/IGARSS46834.2022.9884244

Ahmed, O. S., Franklin, S. E., Wulder, M. A., White, J. C. (2015). Characterizing stand-level forest canopy cover and height using Landsat time series, samples of airborne lidar, and the random forest algorithm. *ISPRS Journal of Photogrammetry and Remote Sensing*, 101, 89-101. https://doi.org/10.1016/j.isprsjprs.2014.11.007

Andreo, V., Dogliotti, A. I., Tauro, C., Neteler, M. (2015). Spatio-temporal variations in chlorophyll-a concentration in the patagonic continental shelf: An example of satellite time series processing with GRASS GIS temporal modules. *2015 IEEE International Geoscience And Remote Sensing Symposium (IGARSS)*, 2249-2252. https://doi.org/10.1109/IGARSS.2015.7326254

Ayhan, E., Kansu, O. (2012). Analysis of Image Classification Methods for Remote Sensing. *Experimental Techniques*, 36, 1, 18-25. https://doi.org/10.1111/j.1747-1567.2011.00719.x

Bakr, N., Weindorf, D., Bahnassy, M., Marei, S., El-Badawi, M. (2010). Monitoring land cover changes in a newly reclaimed area of Egypt using multi-temporal Landsat data. *Applied Geography*, 30, 4, 592-605. https://doi.org/10.1016/j.apgeog.2009.10.008

Collins, L., McCarthy, G., Mellor, A., Newell, G., Smith, L. (2020). Training data requirements for fire severity mapping using Landsat imagery and random forest. *Remote Sensing of Environment*, 245, 111839, https://doi.org/10.1016/j.rse.2020.111839

Cuartero, A., Paoletti, M. E., Presas, A. R., Haut, J. M. (2022). Bi-Dimensional Vector Data Analysis of Positional Accuracy of Landsat-8 Image with Pycircularstats. *IGARSS 2022 – 2022 IEEE International Geoscience And Remote Sensing Symposium*, 2442-2445. https://doi.org/10.1109/IGARSS46834.2022.9883588

De Sarkar, A., Biyahut, N., Kritika, S., Singh, N. (2012). An environment monitoring interface using GRASS GIS and Python. *2012 3rd International Conference On Emerging Applications of Information Technology*, 235-238. https://doi.org/10.1109/EAIT.2012.6407912

Dewali, S. K., Jain, K., Varshney, D., Dhamija, S., Pundir, E. (2023). Combining OBIA, CNN, and UAV photogrammetry for automated avalanche deposit detection and characterization. *Advances in Space Research*, 72, 8, 3109-3132. https://doi.org/10.1016/j.asr.2023.06.033

dos Santos Luciano. A. C., Picoli, M. C. A., Duft, D. G., Rocha, J. V., Leal, M. R. L. V., le Maire, G. (2021). Empirical model for forecasting sugar-cane yield on a local scale in Brazil using Landsat imagery and a random forest algorithm. *Computers and Electronics in Agriculture*, 184, 106063. https://doi.org/10.1016/j.compag.2021.106063

dos Santos Luciano, A. C., Picoli, M. C. A., Rocha, J. V., Duft, D. G., Lamparelli, R. A. C., Leal, M. R. L. V., Le Maire. G. (2019). A generalized space-time OBIA classification scheme to map sugarcane areas at regional

scale, using Landsat images time-series and the random forest algorithm. *International Journal of Applied Earth Observation and Geoinformation*, 80, 127-136. https://doi.org/10.1016/j.jag.2019.04.013

Fisher, J. R. B., Acosta, E. A., Dennedy-Frank, P. J., Kroeger, T., Boucher, T. M. (2018). Impact of satellite imagery spatial resolution on land use classification accuracy and modeled water quality. *Remote Sensing in Ecology and Conservation*, 4, 2, 137-149. https://doi.org/10.1002/rse2.61

Fox, V. E., Lindeque, P. M., Simmons, R. E., Berry, H. H., Brain, C., Brabys, R. (1997). Flamingo 'rescue' in Etosha National Park, 1994: technical, conservation and economic considerations. *Ostrich*, 68, 2-4, 72-76. https://doi.org/10.1080/00306525.1997.9639715

Gargallo, E. (2020). Community conservation and land use in Namibia: Visions, expectations and realities. *Journal of Southern African Studies*, 46, 1, 129–147. https://doi.org/10.1080/03057070.2020.1705617

Ghosh, A., Sharma, R., Joshi, P. (2014). Random forest classification of ur- ban landscape using Landsat archive and ancillary data: Combining seasonal maps with decision level fusion. *Applied Geography*, 48, 31-41. https://doi.org/10.1016/j.apgeog.2014.01.003

Goldblatt, R., Stuhlmacher, M. F., Tellman, B., Clinton, N., Hanson, G., Georgescu, M., Balling, R. C. (2018). Using Landsat and nighttime lights for supervised pixel-based image classification of urban land cover. *Remote Sensing of Environment*, 205, 253-275. https://doi.org/10.1016/j.rse.2017.11.026

GRASS Development Team (2022). *Geographic Resources Analysis Support System (GRASS GIS) Software, Version 8.2* [Computer software manual]. Retrieved from https://grass.osgeo.org

Grinand, C., Rakotomalala, F., Gond, V., Vaudry, R., Bernoux, M., Vieilledent, G. (2013). Estimating deforestation in tropical humid and dry forests in Madagascar from 2000 to 2010 using multi-date Landsat satellite images and the random forests classifier. *Remote Sensing of Environment*, 139, 68-80. https://doi.org/10.1016/j.rse.2013.07.008

Gupta, R., Kumar, S., Gupta, A. (2022). Application of Convolution Neural Network for Cloud Shadows Removal in Landsat Imagery. *2022 IEEE International Conference On Current Development in Engineering and Technology (CCET)*, 1-8. https://doi.org/10.1109/CCET56606.2022.10080513

Berry, H. H., Fox, V. E., Berry, P. E. (2001). Synchrony of drinking in Double-banded Sandgrouse, Pterocles bicinctus, at Etosha National Park, Namibia. *Ostrich*, 72, 1–2, 109-113. https://doi.org/10.2989/00306520109485294

Himmelsbach, T., Beyer, M., Wallner, M., Grünberg, I., Houben, G. (2018). Deep, semi-fossil aquifers in southern Africa: A synthesis of hydrogeological investigations in northern Namibia. *Biodiversity & Ecology*, 6, 66–74. https://doi.org/10.7809/b-e.00306

Hofierka, J., Mitášová, H., Neteler, M. (2009). Chapter 17 Geomorphometry in GRASS GIS. In: T. Hengl & H. I. Reuter (Eds.), *Geomorphometry*, 33, 387–410. https://doi.org/10.1016/S0166-2481(08)00017-2

Inzana, J., Kusky, T., Higgs, G., Tucker, R. (2003). Supervised classifications of Landsat TM band ratio images and Landsat TM band ratio image with radar for geological interpretations of central Madagascar. *Journal of African Earth Sciences*, 37, 1, 59-72. https://doi.org/10.1016/S0899-5362(03)00071-X

Jasiewicz, J. (2011). A new GRASS GIS fuzzy inference system for massive data analysis. *Computers & Geosciences*, 37, 9, 1525–1531. https://doi.org/10.1016/j.cageo.2010.09.008

Jasiewicz, J., Metz, M. (2011). A new GRASS GIS toolkit for Hortonian analysis of drainage networks. *Computers & Geosciences*, 37, 8, 1162–1173. https://doi.org/10.1016/j.cageo.2011.03.003

Koeniger, P., Hamutoko, J., Post, V. E. A., Beyer, M., Gaj, M., Himmelsbach, T., Wanke, H. (2021). Evaporation loss along the Calueque-Oshakati Canal in the Cuvelai-Etosha Basin (Northern Namibia): evidence from stable isotopes and hydrochemistry. *Isotopes in Environmental and Health Studies*, S 57, 1, 53–66. https://doi.org/10.1080/10256016.2020.1830082

Lemenkova, P. (2022a). Console-Based Mapping of Mongolia Using GMT Cartographic Scripting Toolset for Processing TerraClimate Data. *Geosciences*, 12, 140, 1–36. https://doi.org/10.3390/geosciences12030140

Lemenkova, P. (2022b). Mapping Climate Parameters over the Territory of Botswana Using GMT and Gridded Surface Data from TerraClimate. *ISPRS International Journal of Geo-Information*, 11, 473. https://doi.org/10.3390/ijgi11090473

Lemenkova, P. (2023a). A GRASS GIS Scripting Framework for Monitoring Changes in the Ephemeral Salt Lakes of Chotts Melrhir and Merouane, Algeria. *Applied System Innovation*, 6, 61. https://doi.org/10.3390/asi6040061
Lemenkova, P. (2023b). Image Segmentation of the Sudd Wetlands in South Sudan for Environmental Analytics by GRASS GIS Scripts. *Analytics*, 2, 745-780. https://doi.org/10.3390/analytics2030040
Lemenkova, P. (2023c). Monitoring Seasonal Fluctuations in Saline Lakes of Tunisia Using Earth Observation Data Processed by GRASS GIS. *Land*, 12, 1995. https://doi.org/10.3390/land12111995
Lemenkova, P. (2023d). Using open-source software GRASS GIS for analysis of the environmental patterns in Lake Chad, Central Africa. *Die Bodenkultur: Journal of Land Management, Food and Environment*, 74, 1, 49-64. https://doi.org/10.2478/boku-2023-0005
Lemenkova, P. (2024a). Deep Learning Methods of Satellite Image Processing for Monitoring of Flood Dynamics in the Ganges Delta, Bangladesh. *Water*, 16, 8, 1141. https://doi.org/10.3390/w16081141
Lemenkova, P. (2024b). Random Forest Classifier Algorithm of Geographic Resources Analysis Support System Geographic Information System for Satellite Image Processing: Case Study of Bight of Sofala, Mozambique. *Coasts*, 4, 1, 127-149. https://doi.org/10.3390/coasts4010008
Lemenkova, P. (2024c). Artificial Neural Networks for Mapping Coastal Lagoon of Chilika Lake, India, Using Earth Observation Data. *Journal of Marine Science and Engineering*, 12, 5, 709. https://doi.org/10.3390/jmse12050709
Lemenkova, P. (2024d). An automated algorithm of GRASS GIS to retrieve the data on land cover types in Guinea, West Africa, from Landsat-8 OLI/TIRS images. *Ovidius University Annals of Constanta - Series Civil Engineering*, 25, 1, 19-36. https://doi.org/10.2478/ouacsce-2025-0005
Lu, S., Bian, Y., Chen, F., Lin, J., Lyu, H., Li, Y., Lyu, L. (2023). An operational approach for large-scale mapping of water clarity levels in inland lakes using Landsat images based on optical classification. *Environmental Research*, 237, 116898. https://doi.org/10.1016/j.envres.2023.116898
Luetkemeier, R., Stein, L., Drees, L., Liehr, S. (2017). Blended Drought Index: Integrated Drought Hazard Assessment in the Cuvelai-Basin. Climate, Mao D., Wang, Z., Du, B., Li, L., Tian, Y., Jia, M., Wang, Y. (2020). National wetland mapping in China: A new product resulting from object-based and hierarchical classification of Landsat 8 OLI images. *ISPRS Journal of Photogrammetry and Remote Sensing*, 164, 11-25. https://doi.org/10.1016/j.isprsjprs.2020.03.020
Martínez-Montoya, J., Herrero, J., Casterad, M. (2010). Mapping categories of gypseous lands in Mexico and Spain using Landsat imagery. *Journal of Arid Environments*, 74, 8, 978-986. https://doi.org/10.1016/j.jaridenv.2010.01.011
McKee, J., Weber, E. (2021). Effect of Image Classification Accuracy on Dasymetric Population Estimation. Urban remote sensing, 283-304. https://doi.org/10.1002/9781119625865.ch13
Melville, B., Lucieer, A., Aryal, J. (2018). Object-based random forest classification of Landsat ETM+ and WorldView-2 satellite imagery for mapping lowland native grassland communities in Tasmania, Australia. *International Journal of Applied Earth Observation and Geoinformation*, 66, 46-55. https://doi.org/10.1016/j.jag.2017.11.006
Hipondoka, M. H. T., van der Waal, B. C. W., Ndeutapo, M. H., Hango, L. (2018). Sources of fish in the ephemeral western iishana region of the Cuvelai–Etosha Basin in Angola and Namibia. *African Journal of Aquatic Science*, 43, 3, 199-214. https://doi.org/10.2989/16085914.2018.1506310
Miller, R. M., Pickford, M., Senut, B. (2010). The Geology, Palaeontology and Evolution of the Etosha Pan, Namibia: Implications for Terminal Kalahari Deposition. *South African Journal of Geology*, 113, 3, 307-334. https://doi.org/10.2113/gssajg.113.3.307
Mulik, M. B., Jayashree, V., Kulkarni, P. N. (2023). Reflectance material classification using optimized deep learning and change detection of LANDSAT surface reflectance images. *Engineering Applications of Artificial Intelligence*, 126, 106697. https://doi.org/10.1016/j.engappai.2023.106697
Murthy, T. S. D., Aryalekshmi, B. N., Nayana, D. K. (2023). District-Level Vegetation and Wetland Analysis with GEE Python API: A Flask Web Application Approach. 2023 7th International Conference on Computa-

tion System and Information Technology for Sustainable Solutions (CSITSS), 1-6. https://doi.org/10.1109/CSITSS60515.2023.10334172

Nguyen, M. H., Li, J., Crawl, D., Block, J., Altintas, I. (2019). Scaling Deep Learning-Based Analysis of High-Resolution Satellite Imagery with Distributed Processing. *2019 IEEE International Conference On Big Data (big data)*, 5437-5443. https://doi.org/10.1109/BigData47090.2019.9006205

Novelli, M., Gebhardt, K. (2007). Community based tourism in Namibia: 'reality show' or 'window dressing'? *Current Issues in Tourism*, 10, 5, 443–479. https://doi.org/10.2167/cit332.0

Oliphant, A. J., Thenkabail, P. S., Teluguntla, P., Xiong, J., Gumma, M. K., Congalton, R. G., Yadav, K. (2019). Mapping cropland extent of Southeast and Northeast Asia using multi-year time-series Landsat 30-m data using a random forest classifier on the Google Earth Engine Cloud. *International Journal of Applied Earth Observation and Geoinformation*, 81, 110–124. https://doi.org/10.1016/j.jag.2018.11.014

Ousmanou, S., Martial, F. E., Jules, T. K., Ludovic, A. M., Blandine, A. K. T., Sufinatu, A., Maurice, K. (2024). Mapping and discrimination of the mineralization potential in granitoids from Banyo area (Adamawa, Cameroon), using Landsat 9 OLI, ASTER images and field observations. *Geosystems and Geoenvironment*, 3, 1, 100239. https://doi.org/10.1016/j.geogeo.2023.100239

Pedregosa, F., Varoquaux, G., Gramfort, A., Michel, V., Thirion, B. (2011). Scikit-Learn: Machine Learning in Python. *Journal of Machine Learning Research*, 12, 2825–2830.

Phiri, D., Morgenroth, J., Xu, C., Hermosilla, T. (2018). Effects of pre-processing methods on Landsat OLI-8 land cover classification using OBIA and random forests classifier. *International Journal of Applied Earth Observation and Geoinformation*, 73, 170-178. https://doi.org/10.1016/j.jag.2018.06.014

Preston-Whyte, R. A., Diab, R. D., Sokolic, F. (1994). Thermo-Topographically Induced Winds in The Boundary Layer Over the Etosha Pan. South *African Geographical Journal*, 76, 2, 59–62. https://doi.org/10.1080/03736245.1994.9713576

Simmons, R. E., Barnard, P., Jamieson, I. G. (1999). What precipitates influxes of wetland birds to ephemeral pans in arid landscapes? Observations from Namibia. *Ostrich*, 70, 2, 145–148. https://doi.org/10.1080/00306525.1999.9634531

Rocchini, D., Delucchi, L., Bacaro, G., Cavallini, P., Feilhauer, H., Foody, G. M., Neteler, M. (2013). Calculating landscape diversity with information-theory based indices: A GRASS GIS solution. *Ecological Informatics*, 17, 82-93. https://doi.org/10.1016/j.ecoinf.2012.04.002

Rocchini, D., Petras, V., Petrasova, A., Chemin, Y., Ricotta, C., Frigeri, A., Neteler, M. (2017). Spatio-ecological complexity measures in GRASS GIS. *Computers & Geosciences*, 104, 166-176. https://doi.org/10.1016/j.cageo.2016.05.006

Roux, C. L. (1979). The grazing capacity of the plains in the Etosha National Park. *Proceedings of the Annual Congresses of the Grassland Society of Southern Africa*, 14, (1), 89-93. https://doi.org/10.1080/00725560.1979.9648866

Shahrin, F., Zahin, L., Rahman, R., Hossain, A. J., Kaf, A. H., Abdul Malek Azad, A. (2020). Agricultural Analysis and Crop Yield Prediction of Habiganj using Multispectral Bands of Satellite Imagery with Machine Learning. *2020 11th International Conference On Electrical And Computer Engineering (ICECE)*, 21-24. https://doi.org/10.1109/ICECE51571.2020.9393066

Shih, F. Y., Chen, G. P. (1994). Classification of Landsat remote sensing images by a fuzzy unsupervised clustering algorithm. *Information Sciences – Applications*, 1, 2, 97-116. https://doi.org/10.1016/1069-0115(94)90010-8

Singh, R. K., Singh, P., Drews, M., Kumar, P., Singh, H., Gupta, A. K., Kumar, M. (2021). A machine learning-based classification of LANDSAT images to map land use and land cover of India. *Remote Sensing Applications: Society and Environment*, 24, 100624. https://doi.org/10.1016/j.rsase.2021.100624

Strigaro, D., Moretti, M., Mattavelli, M., Frigerio, I., Amicis, M. D., Maggi, V. (2016). A grass gis module to obtain an estimation of glacier behavior under climate change: A pilot study on Italian glacier. *Computers & Geosciences*, 94, 68-76. https://doi.org/10.1016/j.cageo.2016.06.009

Teluguntla, P., Thenkabail. P. S., Oliphant, A., Xiong, J., Gumma, M. K., Congalton. R. G., Huete, A. (2018). A 30-m Landsat-derived cropland extent product of Australia and China using random forest machine

learning algorithm on Google Earth Engine cloud computing platform. *ISPRS Journal of Photogrammetry and Remote Sensing*, 144, 325-340. https://doi.org/10.1016/j.isprsjprs.2018.07.017

Upadhyay, A., Shetty, A., Kumar Singh, S., Siddiqui, Z. (2016). Land use and land cover classification of LISS-III satellite image using KNN and decision tree. *2016 3rd International Conference On Computing For Sustainable Global Development*, 1277-1280.

Wagenseil. H., Samimi, C. (2006). Assessing spatio-temporal variations in plant phenology using fourier analysis on NDVI time series: results from a dry savannah environment in Namibia. *International Journal of Remote Sensing*, 27, 16, 3455-3471. https://doi.org/10.1080/01431160600639743

Wang, X., Wen, Z., Liu, G., Tao, H., Song, K. (2022). Remote estimates of total suspended matter in China's main estuaries using Landsat images and a weight random forest model. *ISPRS Journal of Photogrammetry and Remote Sensing*, 183, 94-110. https://doi.org/10.1016/j.isprsjprs.2021.11.001

Wei, J., Huang, W., Li, Z., Sun, L., Zhu, X., Yuan, Q., Cribb, M. (2020). Cloud detection for Landsat imagery by combining the random forest and superpixels extracted via energy-driven sampling segmentation approaches. *Remote Sensing of Environment*, 248, 112005. https://doi.org/10.1016/j.rse.2020.112005

Wessel, P., Luis, J. F., Uieda, L., Scharroo, R., Wobbe, F., Smith, W. H. F., Tian, D. (2019). The Generic Mapping Tools Version 6. *Geochemistry, Geophysics, Geosystems*, 20, 11, 5556-5564. https://doi.org/10.1029/2019GC008515

Yadav, A., Saraswat, S., Faujdar, N. (2022). Geological Information Extraction from Satellite Imagery Using Machine Learning. *2022 10th International Conference on Reliability, Infocom Technologies and Optimization (Trends And Future Directions) (ICRITO)*, 1-5. https://doi.org/10.1109/ICRITO56286.2022.9964623

Yoo, C., Han, D., Im, J., Bechtel, B. (2019). Comparison between convolutional neural networks and random forest for local climate zone classification in mega urban areas using Landsat images. *ISPRS Journal of Photogrammetry and Remote Sensing*, 157, 155-170. https://doi.org/10.1016/j.isprsjprs.2019.09.009

Zhang, M., Zhang, H., Yao, B., Lin, H., An, X., Liu, Y. (2023). Spatiotemporal changes of wetlands in China during 2000–2015 using Landsat imagery. *Journal of Hydrology*, 621, 129590. https://doi.org/10.1016/j.jhydrol.2023.129590

CONFLICTS OF INTEREST

The author declared no potential conflicts of interest with respect to the research, authorship, and/or publication of this article.

ORCID Polina Lemenkova: https://orcid.org/0000-0002-5759-1089